Desalination and Water Treatment
www.deswater.com
doi: 10.5004/dwt.2020.25424

185 (2020) 355–363
May

Removal of methylene blue by NaX zeolites synthesized from coal gasification fly ash using an alkali fusion-hydrothermal method

Yun-Peng Zhao[a,*], Dong-Xue Guo[a], Shi-Feng Li[b], Jing-Pei Cao[a,*], Xian-Yong Wei[a]

[a]*Key Laboratory of Coal Processing and Efficient Utilization (Ministry of Education), China University of Mining & Technology, Xuzhou 221116, China, Tel. +86 516 83885951; Fax: 86 516 83591093; email: zhaoyp@cumt.edu.cn (Y. Zhao), Tel. +86 516 83885951; emails: caojingpei@cumt.edu.cn (J.-P. Cao), 704937207@qq.com (D.-X. Guo), wei_xianyong@163.com (X.-Y. Wei)*
[b]*College of Chemical Engineering, Shenyang University of Chemical Technology, Shenyang 110142, China, email: li.shi.feng@163.com (S.-F. Li)*

Received 3 June 2019; Accepted 1 January 2020

ABSTRACT

NaX zeolites were prepared via an alkali fusion-hydrothermal method from coal gasification fly ash. The effects of the adsorbent dosages, initial dye concentrations, adsorption temperatures and pH values on the adsorption capacity of methylene blue (MB) onto the NaX zeolites were evaluated in batch mode. The maximum adsorption capacity of MB onto the NaX zeolites is 127.13 mg/g, which is higher than the recently reported values using similar adsorbents. The adsorption isotherm data fitted well to the Langmuir model, and the adsorption kinetics followed the pseudo-second-order model. Negative changes in Gibbs free energy ($\Delta G°$) and enthalpy ($\Delta H°$), and a positive change in entropy ($\Delta S°$), suggested that the adsorption of MB onto the NaX zeolites is an exothermic and spontaneous process.

Keywords: Zeolite; Fly ash; Methylene blue; Kinetics; Adsorption isotherm

1. Introduction

Dyestuff wastewaters generated in several industries, such as the food, paper, textile, pulp mill, leather and plastic industries, have caused severe problems for the environment and public health [1–5]. The dyes, even at trace levels, can lead to significant environmental pollution. For instance, dyes can deteriorate water quality by spreading odor and color contaminants, blocking sunlight and impairing the photosynthesis of aquatic plants [6]. Moreover, many dyestuffs in wastewater are toxic or even carcinogenic [7,8].

Methylene blue (MB), a typical cationic dye, is mainly used for dyeing silk, cotton, and wool. MB can cause tachycardia, hyperhemoglobinemia, expiratory dyspnea, spasm, eye burn and skin irritation [9]. In recent decades, MB has been widely studied because of its strong adsorption capacity onto solids, enabling its removal from polluted water [10]. Several methods, such as biodegradation [4], adsorption [11] and photodegradation [12], have been used for the removal of dyes from wastewater. In these reported methods, adsorption is considered to be the most effective method because of its low-cost and nontoxicity [13,14]. Zeolites [15], molecular sieves [16], activated carbon [17] and clay [18] have been applied to adsorb dyes from contaminated water.

As a by-product of coal power plants and gasification plants, fly ash (FA) occupies a large amount of cultivated land and consumes a considerable amount of ash-removing water. In addition, the secondary dust of FA is harmful to the ecological environment [19,20]. Extensive measures have been taken for the long-term use of FA due to the increasing conflict

* Corresponding authors.

between international energy demand and environmental protection. The conversion of FA to zeolites was considered a promising method is given that amorphous aluminosilicate is the major component of FA (approximately 80%) [21–25].

There are two methods, one-step and two-step processes using solid wastes such as silica-alumina to synthesize zeolite materials. The one-step process, such as the traditional hydrothermal synthesis [26], aims to synthesize zeolites from the whole solid silica without any pretreatment. However, the crystals of FA, such as quartz and mullite, are difficult to dissolve in alkali solutions. In contrast, the two-step method, such as two-step hydrothermal synthesis [27], requires the separation of solid residue after dissolving most of the silica and alumina in the alkali solution. Ruen-ngam et al. [28] proposed a new synthesis process by introducing an alkaline fusion step prior to the traditional synthesis process of zeolites, known as the fusion method. This method significantly improved the zeolitization process, affording single-phase and high-crystalline zeolites such as zeolites A and X. To our knowledge, FA-derived zeolite is an effective sorbent to adsorption heavy metals from wastewater, but the use of FA-derived zeolite synthesized by a fusion method in the removal of organic cationic dyes have rarely been investigated.

In the present work, the NaX zeolites were synthesized from coal gasification FA by an alkali fusion-hydrothermal method. The removal behaviors of MB onto NaX zeolites were investigated as well as their adsorption isotherm, kinetics, and thermodynamics. The results showed that the adsorption capacities of MB onto the NaX zeolites are obviously higher than the recently reported values using similar adsorbents.

2. Experimental setup

2.1. Materials

The FA used in this work was obtained from a gasifier of the Longyu Coal Chemical industry in Yongcheng city, Henan Province, China. Analytical grade sodium hydroxide was purchased from Xiqiao Chemical Co. Ltd, (Foshan city, China). Hydrochloric acid and MB were purchased from Sinopharm group chemical reagent Co. Ltd (Beijing, China).

2.2. Preparation of NaX zeolites

A fusion method followed by a hydrothermal treatment was used to synthesize the NaX zeolites. Briefly, sodium hydroxide was ground and mixed with FA to in a sodium hydroxide mass ratio of 1:1, 1:1.5, and 1:2. The above mixtures were added to a porcelain boat and then fused in a furnace for 60 min at temperatures varying from 550°C to 750°C. Afterward, the fused mixtures were ground into a powder and mixed with deionized water at a mass ratio of 1:8 (fused mixtures: water) affording slurries. The slurries were stirred constantly at 300 rpm for 2 h at room temperature, and then added to a Teflon hydrothermal reactor and crystallized at 60°C–120°C for 12–48 h to afford crystals. Finally, the crystals were filtered and washed with deionized water until the pH of the filtrate was reduced to 8–9, and then dried overnight at 105°C affording the NaX zeolites.

2.3. Characterization

The powder X-ray diffraction (XRD) patterns of the FA and NaX zeolites were obtained in the 2θ ranging from 5° to 40° with 2°/min scanning rate using an XRD diffractometer (Simens D5000, Germany) equipped with Kα Cu radiation (λ = 1.54056 Å) at 30 mA and 40 kV. An FEI Quanta TM 250 (FEI Company, USA) scanning electron microscope (SEM) was used to characterize the morphology of the NaX zeolites. The chemical compositions of FA and NaX zeolites were determined by X-ray fluorescence spectrophotometry (Philips, model PW2400, Netherlands). The specific surface area, pore size, and pore volume were determined by an N_2 adsorption-desorption technique using the Brunauer–Emmett–Teller (BET) method. The concentrations of MB in aqueous solutions by an ultraviolet spectrophotometer (TU-1901, Beijing, China).

2.4. Batch adsorption experiments

A storage solution of 1,000 mg/L MB was first prepared, and working solutions were obtained by dilution with deionized water. Adsorption experiments were carried out in a 200 mL beaker containing 100 mL of MB solutions with initial concentrations ranging from 20 to 140 mg/L and 0.1 g of NaX zeolite at 25°C, and pH = 7. To identify the effect of adsorbent dosage on the adsorption capacity of MB, 0.04–0.16 g of NaX zeolite was added, and the mixtures were shaken at room temperature for 24 h. To investigate the effect of pH on the MB adsorption capacity, different pH values (3.0–12.0) of the 100 mg/L MB solution were prepared. The remaining concentrations of MB in the solution after adsorption were determined by a UV-Vis spectrophotometer.

The amount of MB adsorbed at time t, q_t (mg/g), and the adsorption capacity at equilibrium, q_e (mg/g), were determined by Eqs. (1) and (2), respectively, and the removal ratio of MB (η) was calculated by Eq. (3) [29,30].

$$q_t = \frac{\left(C_0 - C_t\right)V}{m} \tag{1}$$

$$q_e = \frac{\left(C_0 - C_e\right)V}{m} \tag{2}$$

$$\eta = \frac{C_0 - C_t}{C_0} \times 100\% \tag{3}$$

where m (g) is the adsorbent dosage and V (L) is the volume of adsorption solution. C_0, C_t, and C_e (mg/L) are the MB concentrations initially, at time t and at adsorption equilibrium, respectively.

2.5. Adsorption isotherm and kinetic models

Adsorption isotherms are used to estimate the maximum adsorption capacity of adsorbed materials and evaluate the suitability of the adsorption process as a unit operation. In addition, the nature of adsorption can be determined from the fit of the isotherm models to the experimental data [30]. There are three typical adsorption isotherm models,

Langmuir, Freundlich, and Dubinin–Radushkevich (D–R) isotherms, which predict the status of adsorbate molecules distributed on the solid/liquid interface and provide the equilibrium adsorption capacity. The equations and parameters of the isotherm models are shown in Table 1.

2.6. Adsorption thermodynamics

To determine the influence of temperature and investigate the feasibility of MB adsorption onto NaX zeolites, experiments were carried out with initial MB concentrations of 100 mg/L at 25°C, 35°C, and 45°C, respectively. Thermodynamic parameters were determined by the following equations [31].

$$K_D = \frac{q_e}{C_e} \tag{4}$$

$$\Delta G = -RT \text{ Ln } K_D \tag{5}$$

$$\text{Ln } K_D = \frac{\Delta S}{R} - \frac{\Delta H}{RT} \tag{6}$$

where K_D, ΔH (kJ/mol), ΔG (kJ/mol), ΔS (J/kmol), T (K) and R (8.314 J/kmol) are the equilibrium partition constant, enthalpy change, Gibbs free energy change, entropy change, temperature, and universal gas constant, respectively. The values of ΔS and ΔH were determined from the slope and intercept of the plot of $\ln K_D$ vs. $1/T$, respectively, and the values of ΔG were determined from the K_D values for each temperature.

Table 1
Linear forms of kinetic and isotherm models

Model	Name	Equation
Isotherm	Langmuir	$q_e = \frac{q_m K_L C_e}{1 + K_L C_e}$ $R_L = \frac{1}{1 + K_L C_0}$
	Freundlich	$q_e = K_F C_e^{1/n_F}$
	Dubinin–Radushkevich	$\ln q_e = \ln q_{DR} - K_{DR} R^2 T^2 \left[\ln\left(1 + \frac{1}{C_e}\right)\right]^2$
Kinetic	Pseudo-first-order	$\ln(q_e - q_t) = \ln q_e - k_1 t$
	Pseudo-second-order	$\frac{t}{q_t} = \frac{1}{k_2 q_e} + \frac{t}{q_e}$

q_e and q_m are the equilibrium and maximum adsorption capacity, respectively; K_L and R_L are Langmuir constant and separation factor, respectively; K_F and n_F are Freundlich constants; k_1 and k_2 are pseudo-first-order and pseudo-second-order adsorption rate constants, respectively.

3. Results and discussion

3.1. Characterization of materials

As shown in Table S1, the SiO_2/Al_2O_3 ratio of the FA was 2.75, providing the possibility to produce faujasite [27]. The XRD patterns showed that FA is an amorphous phase and that the NaX zeolite exhibits good crystallinity without any impurities (Fig. 1). The peaks at 6.09° (111), 9.98° (220), 15.3° (311), 20.08° (440), 21.50° (531), 23.12° (442), 26.6° (642), 30.2° (660), 30.8° (555), 32.98° (664), 34.2° (913) are typical diffraction peaks of NaX zeolite according to the Joint Committee on Powder Diffraction Standards [32–34]. As shown in Fig. 2, the FA particles show a globular shape with a smooth surface, while NaX zeolite particles are octahedral crystal structures.

Fig. S1a shows that the N_2 adsorption and desorption isotherms of both FA and NaX zeolites display a combination of type I and type IV characteristics, implying the presence of micropores and mesopores [35], which is consistent with their pore size distribution curves (Fig. S1b). However, the adsorbed volume of the NaX zeolite is significantly greater than that of FA. Table 2 shows that the total specific surface area of FA is 4.51 m^2/g, while the specific surface area of the NaX zeolite is 556.23 m^2/g, which suggested that NaOH activation with high-temperature calcination opened the previously-inaccessible pores, created new pores and enlarged the original pores in FA.

3.2. Effects of preparation parameters on the crystallinity of NaX zeolite

Fig. 3a shows that the XRD diffraction peak intensities of NaX zeolites increase with the increase of FA/NaOH mass ratio. An increase in the FA/NaOH mass ratio results in a decrease in the mole ratio of Na_2O to $A1_2O_3$ in the silica gel.

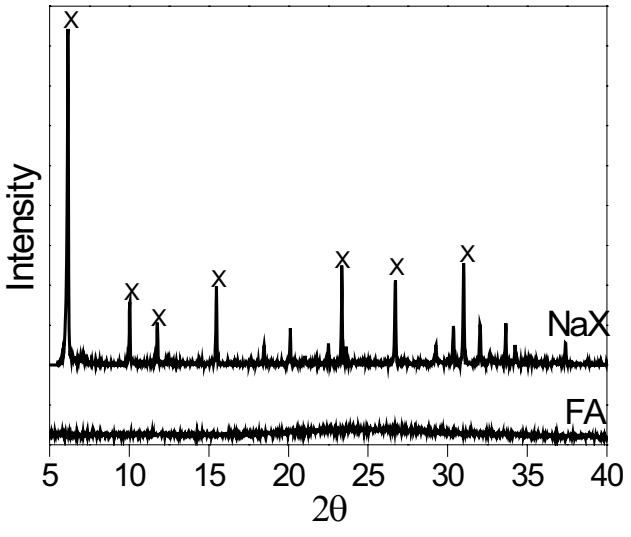

Fig. 1. XRD patterns of FA and NaX zeolite.

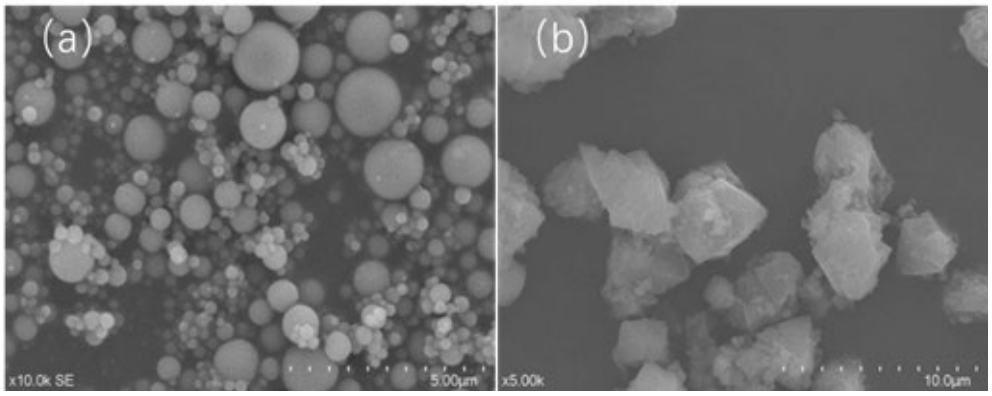

Fig. 2. SEM images of FA (a) and NaX zeolite (b).

Table 2
Textural properties of FA and NaX zeolite

Sample	S_{BET} (m^2/g)	V_{tot} (cc/g)	V_{mec} (cc/g)	Pore size (nm)
FA	4.51	0.025	0.004	22.13
NaX zeolite	556.23	0.345	0.126	2.48

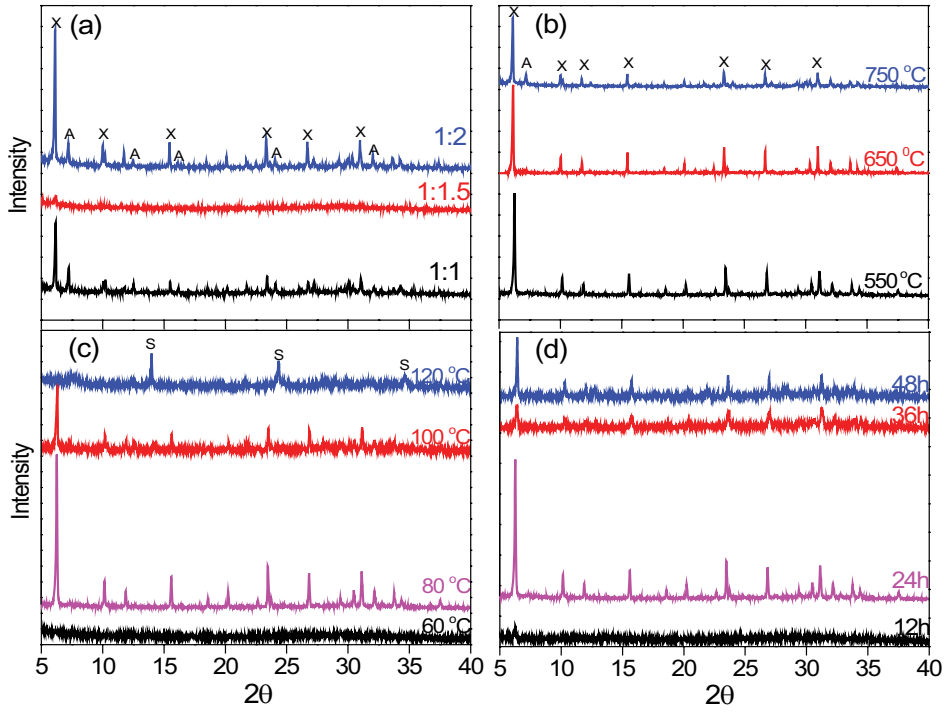

Fig. 3. Effect of the preparation parameters on the crystallinity of NaX zeolites: (a) the mass ratio of FA to NaOH, (b) fusion temperature, (c) crystallization temperature, and (d) crystallization time.

This is conducive to the depolymerization of silicon aluminum gel and an increase in nucleation, resulting in the nucleation rate greater than the crystal growth rate. According to the study of Molina et al. [36], although the high mole ratio of Na_2O to $A1_2O_3$ is beneficial to reduce the particle size, it results in the transcrystallization of zeolites and the formation of other crystalline zeolites.

Fig. 3b shows that the XRD diffraction peak intensities of NaX zeolites decrease with increasing fusion temperature, and a new diffraction peak appears at 750°C. Therefore, the

melting temperature of 550°C is more suitable for the synthesis of NaX zeolite. Fig. 3c shows that the XRD diffraction peak intensity of the NaX zeolite obtained at a crystallization temperature of 80°C is the strongest, and there is a single crystalline phase, indicating that a low temperature is not enough for crystallization, while a high-temperature results in the formation of other crystalline phases. Therefore, the optimum crystallization temperature is 80°C. Fig. 3d shows that the crystallinities of NaX zeolite increase with the reaction time, while the diffraction peak intensities decrease significantly after 24 h of crystallization. Therefore, the optimal crystallization time is 24 h.

3.3. Adsorption of MB onto the NaX zeolites

To determine the optimum dosage of NaX zeolite, a series of experiments were carried out with different amounts of adsorbents (40–160 mg) in 100 mL of 100 mg/L MB solutions at pH = 7. As shown in Fig. 4a, the adsorption capacities of MB decrease and the removal ratios increase with increasing NaX dosage, which is ascribed to the fact that the equilibrium concentrations of MB decrease with increasing zeolite dosage.

As shown in Fig. 4b, the q_e values increase with increasing initial MB concentration. The equilibrium adsorption capacities of MB increase from 20 to 93.95 mg/g when the initial MB concentration ranges from 20 to 140 mg/L. The increase in the initial adsorbate concentration promoted the driving force of mass transfer and the probability of collision between MB and the active sites, resulting in higher adsorption capacity of MB onto zeolite [37].

The pH value of the solution is a crucial factor in the adsorption of dye contaminants [38]. MB is positively charged in solution, therefore, the adsorption capacity of MB increases with increasing pH from 3 to 7, and the maximum adsorption efficiency is 88.17% at pH = 7, while it decreases with increasing pH when the pH value is more than 7 (Fig. 4c). According to the study of Šljivić et al, [39] the pH_{PZC} (point of zero charges) of zeolite is 7.5 in distilled water, and adsorbents will be negatively charged at pH values higher than pH_{PZC} and positively charged at pH values lower than pH_{PZC}. However, the faujasite zeolites, including NaX zeolite, are not stable in strongly acidic media due to the dissolution of Al atoms, causing damage to the zeolitic framework. As shown in Fig. S3, the NaX zeolite still retains a relatively complete octahedral crystal structure after adsorption experiments at pH = 5, while the crystal structure of the NaX zeolite decomposes into an amorphous state after adsorption experiments at pH = 3. These results are similar to those reported by Lin et al [40] and Naudi et al [41].

Due to the decrease in the solution viscosity with increasing temperature, the diffusion rate of adsorbate molecules across the external boundary layer and the internal pores of the adsorbent particle increase with increasing temperature. However, an increase in temperature decreases the equilibrium capacity of a particular adsorbate onto the adsorbent [42]. As shown in Fig. 4d, the adsorption capacity of MB decreases with increasing adsorption temperature. The MB molecules on the surface of the adsorbent are more active at high temperatures, so further increasing temperature favors the desorption of MB.

Table 3 lists the maximum adsorption capacities of the NaX zeolites obtained in this work and previous references [43–48]. The NaX zeolite in this work has a reasonably high

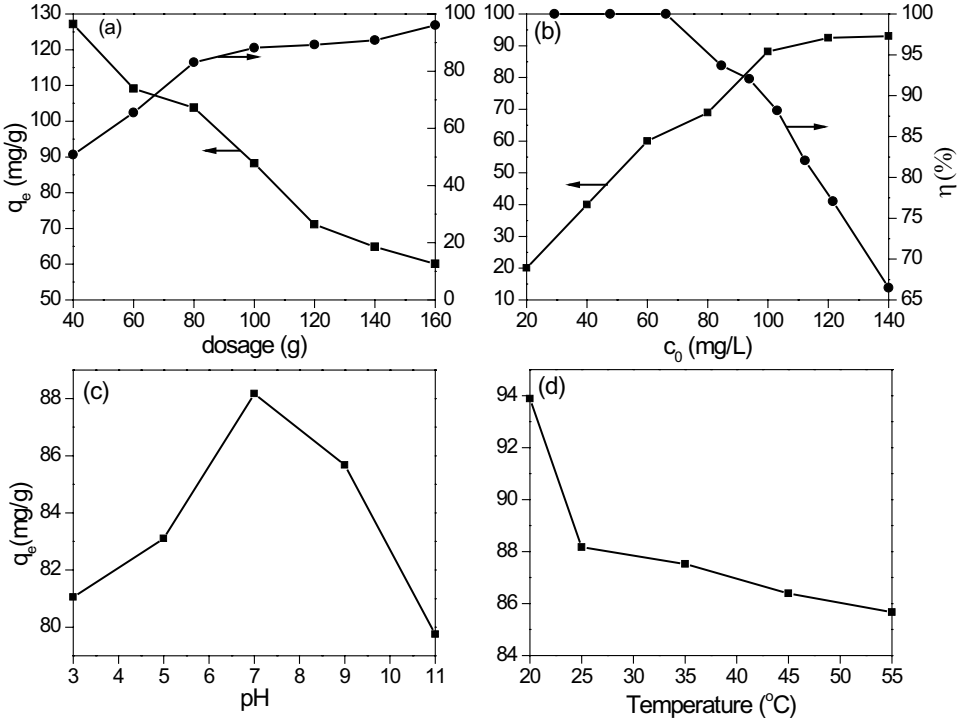

Fig. 4. Effect of adsorption conditions on MB adsorption capacities onto the NaX zeolite: (a) adsorbent dosage, (b) initial MB concentration, (c) pH, and (d) temperature.

adsorption capacity for MB, indicating that it is a potentially excellent adsorbent for MB removal.

3.4. Adsorption isotherm

The Langmuir isotherm model assumes that the adsorption process occurs on a homogeneous surface and that the molecules exhibit an adsorbate monolayer on the surface of adsorbent saturating the pores and preventing transmigration [49]. As shown in Fig. S2, a q_m value of 93.34 mg/g is obtained from the Langmuir isotherm, which is consistent with the experimental value of q_m (93.97 mg/g). The value of R^2 (0.991) indicated that the experimental data were well fitted to the Langmuir isotherm model. As an important parameter of the Langmuir isotherm, the value of the separation factor (R_L) implies the isotherm is irreversible ($R_L = 0$), favorable ($0 < R_L < 1$), linear ($R_L = 1$), or unfavorable ($R_L > 1$) [50]. The values of R_L in the concentration studied (80–140 mg/L) are between 0.044 and 0.025, suggesting that the adsorption process is favorable in the MB-NaX zeolite system. The decrease in the R_L value with increasing initial MB concentration implies that the adsorption is more favorable for adsorption at high concentrations.

The Freundlich isotherm model is an empirical equation used to describe heterogeneous systems with interactions among the molecules adsorbed. The values of the heterogeneity factor (n_F) imply that the adsorption process is physical ($n_F > 1$), linear ($n_F = 1$) or chemical ($n_F < 1$) adsorption [51]. In addition, $1/n_F > 1$ suggests cooperative adsorption, and $1/n_F < 1$ implies a normal Freundlich isotherm. The values of n_F and $1/n_F$ in the MB-NaX zeolite system are 1.45 and 0.69, respectively, indicating that the adsorption of MB onto NaX zeolite occurs by physical adsorption and that the normal Langmuir isotherm is favorable. As shown in Fig. S2, the fitting of the Freundlich isotherm to the experimental data is not very good ($R^2 = 0.973$).

The D–R isotherm provides important information on the free energy involved in the nature of adsorption [52]. The value of R^2 (0.986) for the D–R isotherm is also lower than that for the Langmuir isotherm (Table 4). The value of $K_{D–R}$ (8.89×10^{-5}) indicates that the process of MB adsorption onto the NaX zeolite follows the chemisorption mechanism. Table 4 lists the parameters of the three isotherm models studied for the MB-NaX zeolite system.

3.5. Kinetics studies

Both the pseudo-first-order model and the pseudo-second-order model were applied to simulate the adsorption kinetics of MB onto the NaX zeolite using the data from Fig. 4. The equations of the two models are listed in Table 1. Fig. 5 shows the linear fits of pseudo-first-order and pseudo-second-order models to the MB adsorption. As listed in Table 5, the R^2 value for pseudo-first-order kinetics (0.935) is lower than that for pseudo-second-order kinetics (0.996), and the $q_{e,2cal}$ value is consistent with the experimental value ($q_{e,exp}$). Therefore, the process of MB adsorption onto the NaX zeolite is well fit by the pseudo-second-order kinetics.

Table 3
Adsorption maxima of MB onto various zeolites in literatures

Zeolite material	T (°C)	Adsorptive capacity (mg/g)	Reference
NaX zeolite	25	127.13	This work
Natural zeolite	25	16.37	[43]
Zeolite NaA (purely synthesized)	30	64.80	[44]
ZSM–5 (commercial)	25	8.67	[45]
Zeolite–P2 (purely synthesized)	25	16.86	[46]
MCM–22 (purely synthesized)	30	51.19	[47]
Zeolite synthesized from coal FA	20	37.04–50.51	[48]

Table 4
Parameters of Langmuir and Freundlich isotherm models

Langmuir model			Freundlich model				D–R model	
q_m (mg/g)	K_L (L/mg)	R_L	R^2	K_F (mg/g)(L/mg)$^{1/n}$	n_F	R^2	R^2	$K_{D–R}$
93.34	0.271	0.025–0.044	0.991	37	1.45	0.973	0.986	8.89×10^{-5}

Table 5
Parameters and determination coefficients of the kinetic models for MB adsorption onto NaX zeolite

Pseudo-first-order				Pseudo-second-order		
$q_{e,exp}$ (mg/g)	k_1 (min^{-1})	$q_{e,1cal}$ (mg/g)	R^2	k_2 (min^{-1})	$q_{e,2cal}$ (mg/g)	R^2
88.2	0.0043	74.44	0.935	0.0076	100	0.996

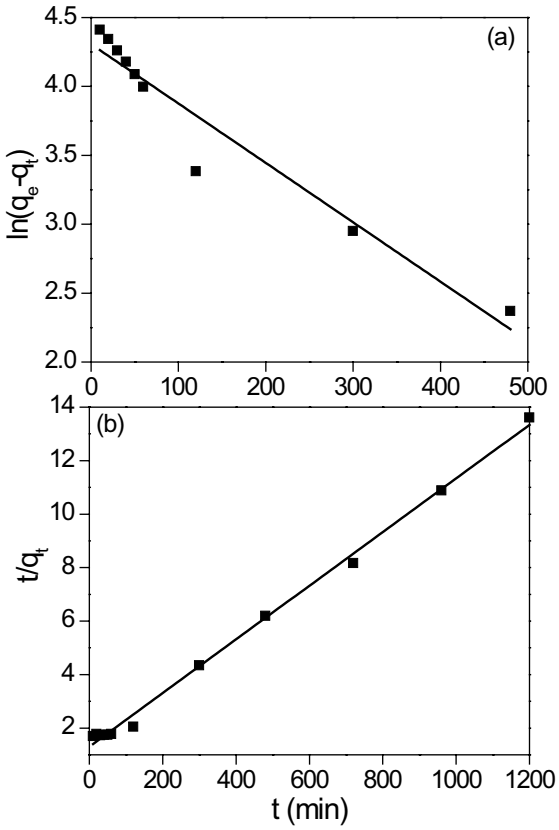

Fig. 5. Linear fits of pseudo-first-order (a) and pseudo-second-order models (b) to the MB adsorption.

Table 6
Thermodynamic parameters for the MB adsorption onto the NaX zeolite

T (°C)	Δ*G* (KJ/mol)	Δ*H* (KJ/mol)	Δ*S* (J/mol k)
25	–75.49		
35	–75.63	–71.33	13.97
45	–75.77		

3.6. Adsorption thermodynamic

As shown in in Fig. S4, the values of Δ*S* and Δ*H* were determined from the intercept and slope of a plot from $\ln K_D$ vs. 1/*T*, and Δ*G* was evaluated using Eq. (4). Table 6 shows that both Δ*H* and Δ*G* were negative, indicating that the adsorption of MB onto the NaX zeolite is exothermic and spontaneous. The positive value of Δ*S* suggested the affinity between MB and the NaX zeolites, and the randomness nature of the adsorption process at the solid/solution interface.

4. Conclusions

NaX zeolites were successfully synthesized from FA by using an alkali fusion-hydrothermal method. The optimal synthetic conditions are as follows: a mass ratio of FA/NaOH, 1:2; activation temperature, 750°C; crystallization temperature, 80°C and crystallization time, 24 h. The synthesized NaX zeolites possess single characteristic peaks, a microporous structure, and a high surface area. The maximum adsorption capacity of MB onto the NaX zeolite is 127.13 mg/g, implying that the NaX zeolite synthesized by the alkali fusion-hydrothermal method from FA can be a good candidate for the treatment of MB-containing wastewater. The adsorption process can be simulated with the Langmuir isotherm model and pseudo-second-order reaction model. Additionally, the adsorption of MB onto the NaX zeolite is a spontaneous and exothermic process.

Acknowledgments

This work was supported by the Fundamental Research Funds for the Central Universities (China University of Mining and Technology, 2017XKZD10).

References

[1] A. Asfaram, M. Ghaedi, G.R. Ghezelbash, Biosorption of Zn^{2+}, Ni^{2+} and Co^{2+} from water samples onto Yarrowia lipolytica ISF7 using a response surface methodology, and analyzed by inductively coupled plasma optical emission spectrometry (ICP-OES), RSC Adv., 6 (2016) 23599–23610.
[2] A. Asfaram, M. Ghaedi, G.R. Ghezelbash, F. Pepe, Application of experimental design and derivative spectrophotometry methods in optimization and analysis of biosorption of binary mixtures of basic dyes from aqueous solutions, Ecotoxicol. Environ. Saf., 139 (2017) 219–227.
[3] E.A. Dil, M. Ghaedi, G.R. Ghezelbash, A. Asfaram, Multi-responses optimization of simultaneous biosorption of cationic dyes by live yeast Yarrowia lipolytica 70562 from binary solution: application of first-order derivative spectrophotometry, Ecotoxicol. Environ. Saf., 139 (2017) 158–164.
[4] G. Crini, Non-conventional low-cost adsorbents for dye removal: a review, Bioresour. Technol., 97 (2006) 1061–1085.
[5] A.R. Bagheri, M. Ghaedi, A. Asfaram, S. Hajati, A.M. Ghaedi, A. Bazrafshan, Modeling and optimization of simultaneous removal of ternary dyes onto copper sulfide nanoparticles loaded on activated carbon using second-derivative spectrophotometry, J. Taiwan Inst. Chem. Eng., 65 (2016) 212–224.
[6] N.R. Rane, V.V. Chandanshive, R.V. Khandare, A.R. Gholave, S.R. Yadav, S.P. Govindwar, Green remediation of textile dyes containing wastewater by *Ipomoea hederifolia*, RSC Adv., 4 (2014) 36623–36632.
[7] K.G. Bhattacharyya, A. Sharma, Kinetics and thermodynamics of methylene blue adsorption on Neem (*Azadirachta indica*) leaf powder, Dyes Pigm., 65 (2005) 51–59.
[8] C.H. Weng, Y.F. Pan, Adsorption of a cationic dye (methylene blue) onto spent activated clay, J. Hazard. Mater., 144 (2007) 355–362.
[9] S. Senthilkumaar, P.R. Varadarajan, K. Porkodi, C.V. Subbhuraam, Adsorption of methylene blue onto jute fiber carbon: kinetics and equilibrium studies, J. Colloid Interface Sci., 284 (2005) 78–82.
[10] B.H. Hameed, A.T.M. Din, A.L. Ahmad, Adsorption of methylene blue onto bamboo-based activated carbon: kinetics and equilibrium studies, J. Hazard. Mater., 141 (2007) 819–825.
[11] E.A. El-Sharkaway, A.Y. Soliman, K.M. Al-Amer, Comparative study for the removal of methylene blue via adsorption and photocatalytic degradation, J. Colloid Interface Sci., 310 (2007) 498–508.
[12] S. Kaur, S. Rani, V. Kumar, R.K. Mahajan, M. Asif, I. Tyagi, Synthesis, characterization and adsorptive application of ferrocene based mesoporous material for hazardous dye Congo red, J. Ind. Eng. Chem., 26 (2015) 234–242.
[13] M.X. Liu, L.H. Gan, Y.C. Pang, Z.J. Xu, Z.X. Hao, L.W. Chen, Synthesis of titania–silica aerogel-like microspheres by a

water-in-oil emulsion method via ambient pressure drying and their photocatalytic properties, Colloids Surf., A, 317 (2008) 490–495.
[14] H. Mazaheri, M. Ghaedi, A. Asfaram, S. Hajati, Performance of CuS nanoparticle loaded on activated carbon in the adsorption of methylene blue and bromophenol blue dyes in binary aqueous solutions: using ultrasound power and optimization by central composite design, J. Mol. Liq., 219 (2016) 667–676.
[15] E.M. Dias, C. Petit, Towards the use of metal–organic frameworks for water reuse: a review of the recent advances in the field of organic pollutants removal and degradation and the next steps in the field, J. Mater. Chem. A, 3 (2015) 22484–22506.
[16] Q.D. Qin, J. Ma, K. Liu, Adsorption of anionic dyes on ammonium-functionalized MCM-41, J. Hazard. Mater., 162 (2009) 133–139.
[17] V. Gomez, M.S. Larrechi, M.P. Callao, Kinetic and adsorption study of acid dye removal using activated carbon, Chemosphere, 69 (2007) 1151–1158.
[18] S.S. Tahir, N. Rauf, Removal of a cationic dye from aqueous solutions by adsorption onto bentonite clay, Chemosphere, 63 (2006) 1842–1848.
[19] X. Querol, N. Moreno, J.C. Umaña, A. Alastuey, E. Hernández, A. López-Soler, Synthesis of zeolites from coal FA: an overview, Int. J. Coal Geol., 50 (2002) 413–23.
[20] Z.K. Zhang, J. Wang, L.N. Liu, B.X. Shen, Preparation and Characterization of glass-ceramics via co-sintering of coal fly ash and oil shale ash-derived amorphous slag, Ceram. Int., 45 (2019) 20058–20065.
[21] X. Querol, N. Moreno, J.C. Umaña, R. Juan, S. Hernández, C. Fernandez-Pereira, Application of zeolite material synthesized from FA to the decontamination of wastewater and flue gas, J. Chem. Technol. Biotechnol., 77 (2002) 292–298.
[22] A.K. Kondru, P. Kumar, T.T. Teng, S. Chand, K.L. Wasewar, Synthesis and characterization of Na-Y zeolite from coal FA and its effectiveness in removal of dye from aqueous solution by wet peroxide oxidation, Arch. Environ. Sci., 5 (2011) 46–54.
[23] R.S. Blissett, N.A. Rowson, A review of the multi-component utilization of coal FA, Fuel, 97 (2012) 1–23.
[24] T.V. Ojumu, P.W. Plessis, L.F. Petrik, Synthesis of zeolite A from coal FA using ultrasonic treatment a replacement for fusion step, Ultrason. Sonochem., 31 (2016) 342–349.
[25] S.S. Bukhari, J. Behin, H. Kazemian, S. Rohani, Effect of ultrasound energy on the zeolitization of chemical extracts from fused coal FA, Ultrason. Sonochem., 28 (2016) 47–53.
[26] N. Murayama, H. Yamamoto, J. Shibata, Mechanism of zeolite synthesis from coal FA by alkai hydrothermal reaction, Int. J. Miner. Process., 64 (2002) 1–7.
[27] G.G. Hollman, G. Steenbruggen, J.M. Janssen, A two-step process for the synthesis of zeolites from coal FA, Fuel, 78 (1999) 1225–1230.
[28] D. Ruen-ngam, D. Rungsuk, R. Apiratikul, P. Pavasant, Zeolite formation from coal FA and its adsorption potential, J. Air Waste Manage., 59 (2009) 1140–1147.
[29] K.C. Bedin, A.C. Martins, A.L. Cazetta, O. Pezoti, V.C. Almeid, KOH-activated carbon prepared from sucrose spherical carbon: adsorption equilibrium, kinetic and thermodynamic studies for Methylene Blue removal, Chem. Eng. J., 286 (2016) 476–484.
[30] K.V. Kumar, V. Ramamurthi, S. Sivanesan, Modeling the mechanism involved during the sorption of Methylene Blue onto FA, J. Colloid Interface Sci., 284 (2005) 14–21.
[31] M. Peydayesh, A. Rahbar-Kelishami, Adsorption of Methylene Blue onto Platanus orientalis leaf powder: kinetic, equilibrium and thermodynamic studies, J. Ind. Eng. Chem., 21 (2015) 1014–1019.
[32] N. Shigemoto, H. Hayashi, Selective formation of NaX zeolite from coal FA by fusion with sodium hydroxide prior to hydrothermal reaction, J. Mater. Sci., 28 (1993) 4781–4786.
[33] P. Panitchakarn, N. Laosiripojana, N. Viriya-umpikul, P. Pavasant, Synthesis of high-purity Na-A and NaX zeolite from coal FA, J. Air Waste Manage., 64 (2014) 586–596.
[34] S. Subhapriya, P. Gomathipriya, Synthesis and characterization of zeolite X from coal fly ash: a study on anticancer activity, Mater. Res. Express, 5 (2018) 401–412.
[35] H.H. Zhao, B.L. Xing, C. Zhang, G.X. Huang, Q.R. Liu, G.Y. Yi, J.B. Jia, M.J. Ma, Z.F. Chen, C.X. Zhang, Efficient synthesis of nitrogen and oxygen co-doped hierarchical porous carbons derived from soybean meal for high-performance supercapacitors, J. Alloys Compd., 766 (2018) 705–715.
[36] A. Molina, C. Poole, A comparative study using two methods to produce zeolite from fly, Miner. Eng., 17 (2004) 167–173.
[37] M. Ghaedi, M.D. Ghazanfarkhani, S. Khodadoust, N. Sohrabi, M. Oftade, Acceleration of methylene blue adsorption onto activated carbon prepared from dross licorice by ultrasonic: equilibrium, kinetic and thermodynamic studies, J. Ind. Eng. Chem., 20 (2014) 2548–2560.
[38] K. Rida, S. Bouraoui, S. Hadnine, Adsorption of methylene blue from aqueous solution by kaolin and zeolite, Appl. Clay Sci., 83–84 (2013) 99–105.
[39] M. Šljivić, I. Smičiklas, S. Pejanović, I. Plećaš, Comparative study of Cu^{2+} adsorption on a zeolite, a clay and a diatomite from Serbia, Appl. Clay Sci., 43 (2009) 33–40.
[40] L.D. Lin, Y. Lin, C.J. Li, D.Y. Wu, H.N. Kong, Synthesis of zeolite/hydrous metal oxide composites from coal FA as efficient adsorbents for removal of methylene blue from water, Int. J. Miner. Process., 148 (2016) 32–40.
[41] B.K. Naudi, A. Goswami, M.K. Purkait, Removal of cationic dyes from aqueous solutions by kaolin: kinetic and equilibrium studies, Appl. Clay Sci., 42 (2009) 583–590.
[42] M. Doğan, M. Alkan, A. Türkyilmaz, Y. Özdemir, Kinetics, and mechanism of removal of methylene blue by adsorption onto perlite, J. Hazard. Mater., 109 (2004) 141–148.
[43] R.P. Han, J.J. Zhang, H. Pan, Y.F. Wang, Z.H. Zhao, M.S. Tang, Study of equilibrium, kinetic and thermodynamic parameters about methylene blue adsorption onto natural zeolite, J. Chem. Eng., 145 (2009) 496–504.
[44] N. Sapawe, A.A. Jalil, S. Triwahyono, M.I.A. Shah, R. Jusoh, N.F.M. Salleh, B.H. Hameed, A.H. Karim, Cost-effective microwave rapid synthesis of zeolite NaA for removal of methylene blue, J. Chem. Eng., 229 (2013) 388–398.
[45] X.Y. Jin, M.Q. Jiang, X.Q. Shan, Z.G. Pei, Z.L. Chen, Adsorption of methylene blue and Orange II onto unmodified and surfactant-modified zeolite, J. Colloid. Interface Sci., 32 (2008) 243–247.
[46] W.T. Tsai, K.J. Hsien, H.C. Hsu, Adsorption of organic compounds from aqueous solution onto the synthesized zeolite, J. Hazard. Mater., 166 (2009) 635–641.
[47] S.B. Wang, H.T. Li, L.Y. Xu, Application of zeolite MCM-22 for basic dye removal from wastewater, J. Colloid Interface Sci., 295 (2006) 71–78.
[48] Z. Sun, C.J. Li, D.Y. Wu, Removal of methylene blue from aqueous solution by adsorption onto zeolite synthesized from coal FA and its thermal regeneration, J. Chem. Technol. Biotechnol., 85 (2010) 845–850.
[49] P.S. Kumar, S. Ramalingam, C. Senthamarai, M. Niranjanaa, P. Vijayalakshmi, S. Sivanesan, Adsorption of dye from aqueous solution by cashew nut shell: studies on equilibrium isotherm, kinetics, and thermodynamics of interactions, Desalination, 261 (2010) 52–60.
[50] K. Mahapatra, D.S. Ramteke, L.J. Paliwal, Production of activated carbon from sludge of food processing industry under controlled pyrolysis and its application for methylene blue removal, J. Anal. Appl. Pyrolysis, 95 (2012) 79–86.
[51] K. Fytianos, E. Voudrias, E. Kokkalis, Sorption–desorption behavior of 2,4-dchlorophenol by marine sediments, Chemosphere, 40 (2000) 3–6.
[52] P.K. Pandey, S.K. Sharma, S.S. Sambi, Removal of lead(II) from wastewater on zeolite-NaX, J. Environ. Chem. Eng., 3 (2015) 2604–2610.

Supplementary information

Table S1
Chemical composition of FA

Major oxides (wt.%)		Trace elemental concentrations (ppm)	
SiO_2	53.77	P	269
Al_2O_3	19.55	Ba	130
CaO	8.23	Sr	106
Fe_2O_3	3.42	S	73
K_2O	2.27	Zn	67
MgO	1.55	Pb	42
Na_2O	1.12	Mn	35
TiO_2	1.09	Zr	25
SiO_2/Al_2O_3	2.75	Cu	22

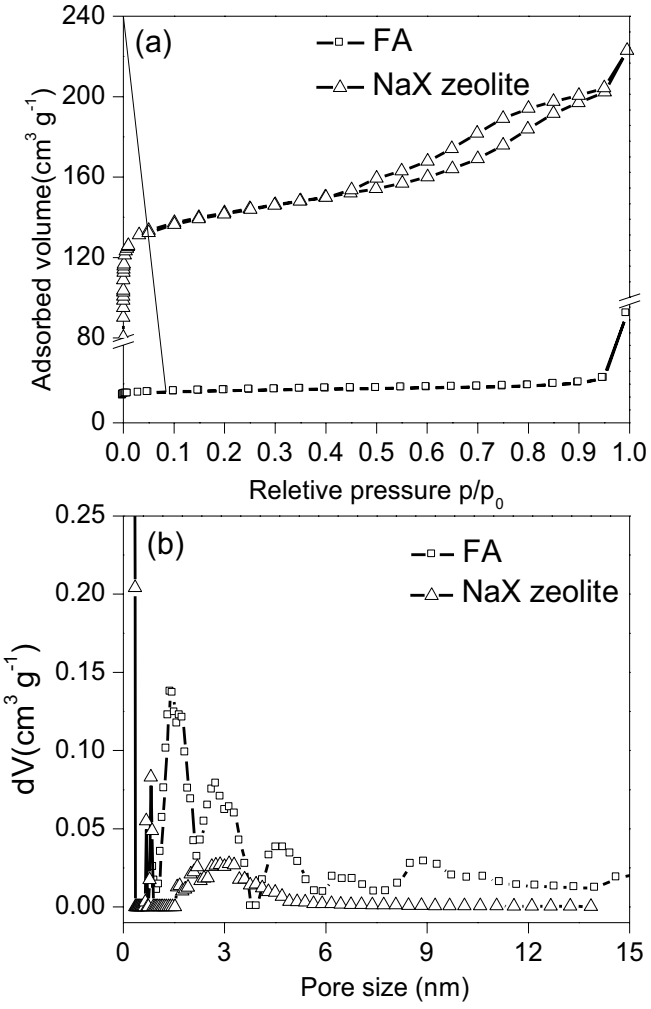

Fig. S1. N_2 adsorption and desorption isotherms at 77 K and pore size distribution of FA and NaX zeolite.

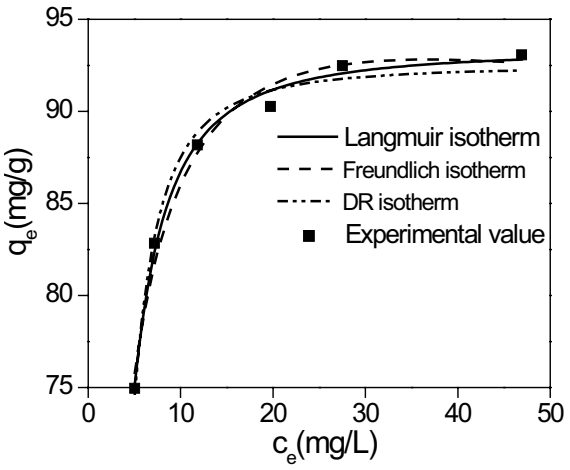

Fig. S2. Adsorption isotherms of MB adsorption onto the NaX zeolite.

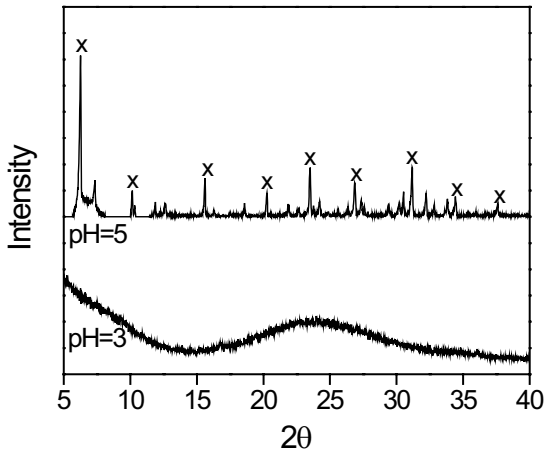

Fig. S3. XRD patterns of the NaX zeolite after adsorption experiments at low pH values.

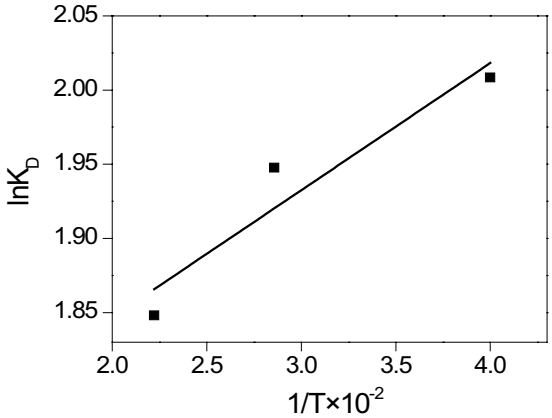

Fig. S4. Thermodynamic linear fitting of MB adsorption onto the NaX zeolite.